MATCHING AND RELATIVE ORIENTATION OF SPHERICAL PANORAMIC IMAGES

Pin-Yun Chen [1], Tsung-Che Huang [2], Yi-Hsing Tseng [3]

Department of Geomatics, National Cheng Kung University, No.1, Daxue Rd., East Dist., Tainan City 70101, Taiwan.

[1]pinyunchen@gmail.com, [2]qaz30162@gmail.com, [3]tseng@mail.ncku.edu.tw

Abstract

People are paying more attention to the use of Spherical Panorama Images (SPIs) for many applications. In order to apply SPIs in photogrammetric application such as land mapping or navigation like frame images do, conjugate points matching and the relative relationship between SPIs are important issues. Through observing the moving pattern of conjugate points, the relative positions and orientation between camera stations may be solved.

In this study, images captured by Ladybug 5 system developed by Point Grey were used for experiment, image features were extracted and matched by Speed-Up Robust Features (SURF) algorithm (Bay, 2008), and the concept of Random Sample Consensus (RANSAC) was applied to improve the accuracy of conjugate points matching.

Although RANSAC general model is not well enough to detect the features on SPIs, we proposed a method using Essential Matrix model to improve this deficiency. Once the conjugate points are found, the relationship between image stations can be explained by Essential matrix, the rotation and translation parts can be extracted up to scale. Similar to that of frame camera, four possible solutions can be found, the angle between two image stations is used to judge the correct solution.

The results show that the quantity and quality of corresponding pairs influences the accuracy of the relative positions and orientations between two images. Although the error matching pair can be found and removed by RANSAC, the distortion comes with projection still make trouble for SURF algorithm. A suitable way is apply image matching on the spherical space to improve quality of corresponding pairs.

Keywords: Image matching, spherical panoramic images, essential matrix, RANSAC

1. INTRODUCTION

1.1. Motivation and Objective

Spherical panoramic image (SPI) has larger field of view than single frame image. An SPI image has larger coverage than a normal one. Consequently, one could use SPIs to have complete coverage with reduced computational cost." Zhang et al (2012) developed an omni-directional 3D camera for robot navigation; Wahbeh et al (2015) applied 3D modelling using panoramic images into an ancient bridge in Ponte Rotto, Rome. This applications all needs large amount of corresponding feature points between SPIs to understand the relationship between them. However, the method of finding corresponding points so far is manually checking, and it is a time-consuming task. In order to apply SPIs in photogrammetric application like frame images do, conjugate points matching and the relative relationship between SPIs are important issues.

Because of complex geometry of SPI, there is a problem to be solved, that is how to ensure the correctness of SPI matching. With the aid from epipolar geometry, lots of applications are proposed such as matching problem, pose problem and so on, it is widely used to establish the relationship between overlapping images. However, the approach is suitable for frame images but failure when applying SPIs since the special sphere geometry.

Corresponding to the two raised problems, there are two objectives in this study. The first one is aims at developing and implementing the theory of SPI matching. With the proposed method, we can increase the efficiency and reliability of matching result. The second one focuses on developing an algorithm to apply epipolar geometry for calculating the position and orientation of the SPIs.

1.2. Research Approach

Image matching plays a key role in deciding correspondences among overlapping image scenes. In this study, Speed-Up Robust Feature (SURF) is applied to extract image features from an SPI, and the descriptors of feature points will be used to search correspondences among SPIs automatically. This makes the precision of SPI matching more robust and reliable for following position and orientation computation.

Then, the relative orientation parameters between two images can be solved by using epipolar geometry. The main problem of this method is the intersection ambiguity. For frame image, there is a solution proposed to solve the problem. This research proposed a novel concept to cope with the problem in SPI case. Applying the proposed method returns a good result. The dominate contribution of this research is that we find out a useful solution for image matching process and get a better results.

2. SPHERICAL PANORAMIC IMAGES

2.1. SPI Geometry

Usually, an SPI is generated by combining a sequence of images captured with a single camera or the images captured with a multi-camera sensor. The geometry of an SPI can be described in Fig. 2.1, where R_{SPI} denotes the spherical radius of an SPI, ρ denotes the zenith angle from the z-axis and α denotes the horizontal angle from the x-axis. Eq. (2.1) formulates the coordinates of an image point defined in the image frame (I-Frame).

Figure 2.1T he SPI spherical coordinate system.

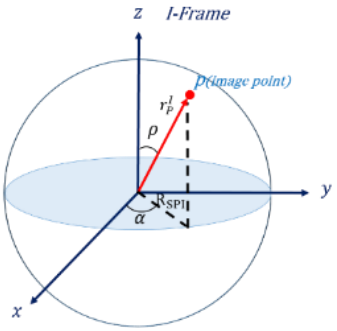

$$r_P^I = \begin{bmatrix} x_p^I \\ y_p^I \\ z_p^I \end{bmatrix} = \begin{bmatrix} R_{SPI} \sin\rho \cos\alpha \\ R_{SPI} \sin\rho \sin\alpha \\ R_{SPI} \cos\rho \end{bmatrix} \quad (2.1)$$

2.2. Exterior Orientation of an SPI

Suppose there is an ideal SPI, the geometric relationship of an image point and the corresponding object point can be described as an image ray. When the image ray is defined in I-Frame and the corresponding object point is defined in object frame, O-Frame, the geometric relationship between the image ray and object point can be described in Fig. 2.2. It means the vector of an object point P is the combination of the vector of SPI centre and the image ray. This relationship can be written as Eq. (2.2).

$$r_P^O = r_I^O + \mathrm{k} \cdot R_I^O \cdot r_P^I \quad (2.2)$$

where,

r_P^O *: the coordinates of object point defined in O-Frame;*

r_I^O *: the coordinates of the SPI center defined in O-Frame;*

R_I^O *: the rotation matrix from I-Frame to O-Frame;*

k *: the scale factor;*

r_P^I *: the coordinates of an object point defined in I-Frame.*

Figure 2.2 The concept of exterior orientation of an SPI.

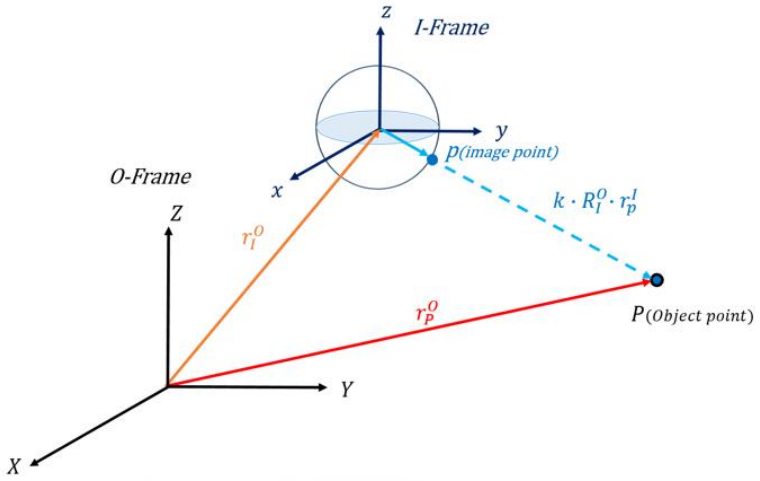

3. RELATIVE ORIENTATION OF AN SPI PAIR

3.1. Relative Orientation

Similar to a stereo pair of frame images, the relative orientation between a pair of overlapping SPIs can be formulated and estimated with conjugate points. Relative orientation defines the position and attitude of one image with respect to the other overlapping image (Ressl, 2000). Assume there are two SPIs, the relative orientation parameters can be written as Eq. (3.1) and Eq. (3.2).

$$r_{I1\to I2}^O = r_{I2}^O - r_{I1}^O \tag{3.1}$$

$$R_{I2}^{I1} = R_O^{I1} R_{I2}^O \tag{3.2}$$

Both translation and rotation include three parameters, so there are totally six elements of relative orientation. However, since the uncertainty of a scale factor, the base vector between two SPIs cannot be determined and the independent parameter is only five. It means that give different scale factors, different translation parameters will be obtained. This will cause the solution infinite if there is no scale factor to be the constraint condition.

Figure 3.1 Concept of relative orientation.

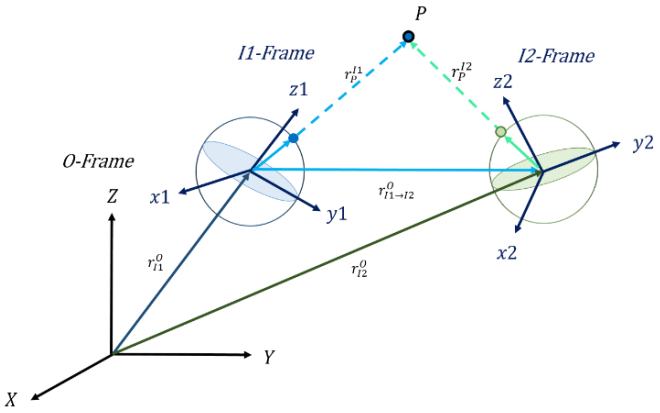

3.2. Estimation of Relative Orientation

The relative orientation between two overlapped SPIs may be retrieved from the essential matrix, and scale factor can be computed with ray intersection method with more SPIs which the E.O parameters are known. To extract the relative orientation parameters, we assume the first camera is at the origin and does not contain rotation, which means I1-Frame equals to O-Frame.

3.2.1. Coplanar Condition

The epipolar geometry can be depicted in Fig 3.2, in which the volume of the parallelepiped is the scalar triple product of the three vectors, namely the image rays of two conjugate points and the base vector, is zero. Eq. (3.3) explains the concept of coplanar condition.

Figure 3.2 Concept of coplanar condition of SPIs.

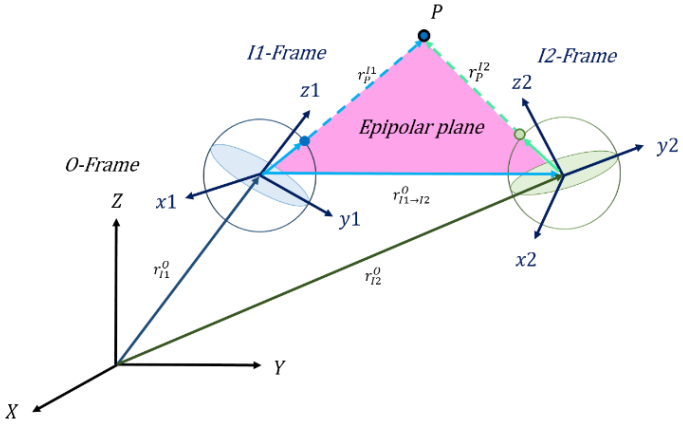

$$(R_{I1}^{O} r_P^{I1})^T \cdot [r_{I1\to I2}^{O} \times R_{I2}^{O} r_P^{I2}] = 0 \tag{3.3}$$

3.2.2. Essential Matrix

Essential matrix describes the relative orientation between two images (Scaramuzza, 2012). Since $(R_{I1}^{O} r_P^{I1})^T$ is equal to $(r_P^{I1})^T R_O^{I1}$, we can rewrite Eq. (3.3) into Eq. (3.4) by using skew-symmetric matrix. Essential matrix is expressed as Eq. (3.5).

$$(r_P^{I1})^T R_O^{I1} \cdot T \cdot R_{I2}^{O} r_P^{I2} = 0 \tag{3.4}$$

where,

$T = \begin{bmatrix} 0 & -\Delta Z & \Delta Y \\ \Delta Z & 0 & -\Delta X \\ -\Delta Y & \Delta X & 0 \end{bmatrix}$: the skew-symmetry matrix of the base vector.

$$E = R_O^{I1} \cdot T \cdot R_{I2}^{O} = \begin{bmatrix} e_{11} & e_{12} & e_{13} \\ e_{21} & e_{22} & e_{23} \\ e_{31} & e_{32} & e_{33} \end{bmatrix} \tag{3.5}$$

The essential matrix can be estimated with matched image features using epipolar constraints described as Eq. (3.4). The minimal case solution involves five 2D to 2D correspondences (Nister, 2004). A simple and straightforward solution is the Longuet-Higgins' eight-point algorithm (Longuet- Hinggins, 1981) which is summarized as Eq. (3.6).

$$\begin{bmatrix} \vdots \\ x_i^{I1}x_i^{I2} \; x_i^{I1}y_i^{I2} \; x_i^{I1}z_i^{I2} \; y_i^{I1}x_i^{I2} \; y_i^{I1}y_i^{I2} \; y_i^{I1}z_i^{I2} \; x_i^{I1}z_i^{I2} \; y_i^{I1}z_i^{I2} \; z_i^{I1}z_i^{I2} \\ \vdots \\ x_n^{I1}x_n^{I2} \; x_n^{I1}y_n^{I2} \; x_n^{I1}z_n^{I2} \; y_n^{I1}x_n^{I2} \; y_n^{I1}y_n^{I2} \; y_n^{I1}z_n^{I2} \; x_n^{I1}z_n^{I2} \; y_n^{I1}z_n^{I2} \; z_n^{I1}z_n^{I2} \end{bmatrix}_{i=1\sim n} \begin{bmatrix} e_{11} \\ e_{12} \\ e_{13} \\ e_{21} \\ e_{22} \\ e_{23} \\ e_{31} \\ e_{32} \\ e_{33} \end{bmatrix} = 0 \tag{3.6}$$

Stacking the constraints from more than eight points gives the linear equation system $AE = 0$. By solving the system, the parameters of E can be computed. A valid essential matrix after SVD is $= U_E D_E V_E^T$, and has $diag(D) = \{d, d, 0\}$, which means that the first and second singular values are equal and the third one is zero. To get a valid essential matrix fulfills the constraint, the solution needs to be projected onto the space. The projected essential matrix is $\bar{E} = U diag\{1, 1, 0\} V^T$.

3.2.3. Ambiguity of Intersection

Four possible solutions are resulted from the ambiguity of intersection. By taking one intersected object point, the ambiguity of intersection in the case of frame images is illustrated in Fig. 3.3 (Hartley et al., 2004). The correct solution can be

confirmed by triangulating a point correspondence in front of both cameras. Fig. 3.3, (a) is the only one correct solution.

Figure 3.3 Intersection ambiguity of frame image (R. Hartley et al., 2004).

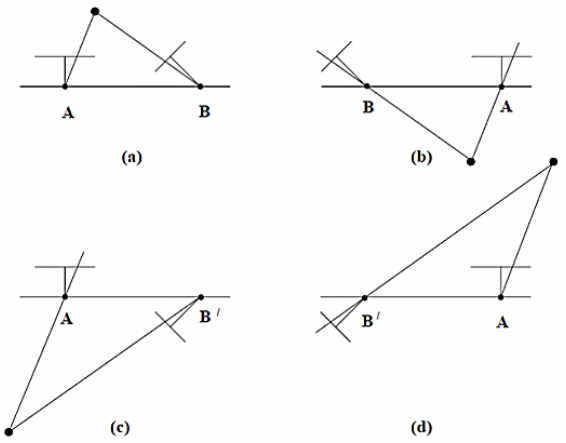

However, the situation become different in SPI case. The approach for frame image is not suitable for SPI since there is no definition of front side and back side for an SPI. In this study, we proposed a novel method to deal with SPI ambiguity. Similar to the frame camera, there are four possible solutions after extracting the rotation and translation from essential matrix. The rotation and translation ambiguity for SPI is illustrated in Fig 3.4.

Figure 3.4 Intersection ambiguity of SPI.

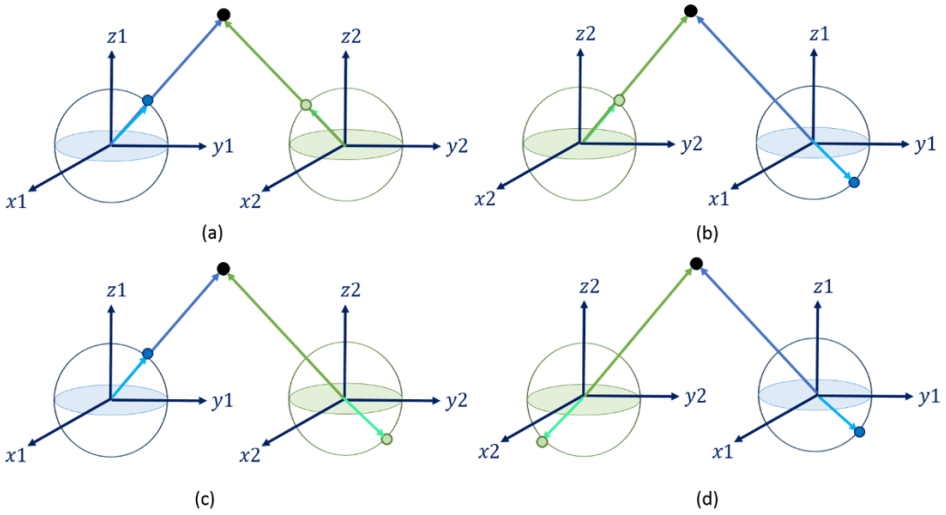

Figure 3.5 shows r_P^I can be transformed into O-Frame by using rotation matrix R_I^O. Vector $r_{I\to P}^O$ also can be computed since we know the position of SPI centre and the point. If both rotation and translation of second camera are correct, the angle between $(R_I^O \cdot r_P^I)$ and $r_{I\to P}^O$ will be close to zero rather than close to 180˚. We can use this check angle to solve the ambiguity of intersection. The only one correct solution is the one has the both check angles of the two SPIs to be small. The check angle of each SPI can be computed by using inner product computation.

Figure 3.6 The check angle relationship for the ambiguity problem.

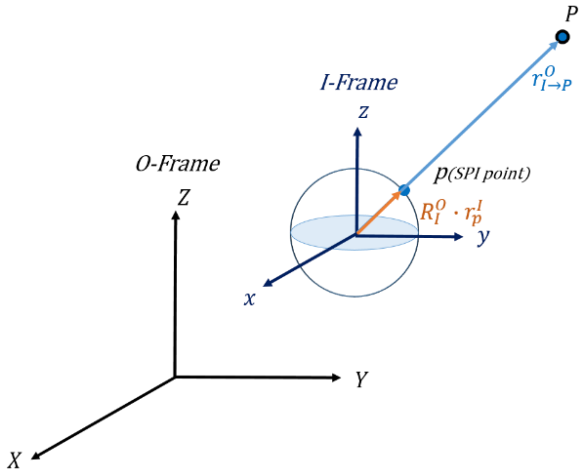

4. IMAGE MATCHING

4.1. Speed-Up Robust Features (SURF) Algorithm

SURF is a scale-invariant and rotation invariant image matching algorithm. Bay et al. (2008) utilize Hessian matrix to detect the feature points at different scale, and utilizes the Haar wavelet responses (Lienhart et al., 2002) in x and y direction to calculate the orientation of feature points. The parameters in the algorithm can be changed in order to adapt to different cases. Figure 4.1 shows the matching results example.

4.2. Error Matching Detection and Elimination

SURF provides all possible image feature matches, in which incorrect matches are inevitable. Random Sample Consensus (RANSAC) (Fishler et al., 1981) is commonly applied for detecting and removing the error matches. It is an iterative method to estimate parameters of a mathematical model from a set of observed

data which may contain outliers. The input of the algorithm is the matching result of SURF algorithm in this research. RANSAC achieves its goal by repeating the procedure shown in Fig 4.2. This procedure in first dot rectangle repeat in a fixed number of times, each time produces a model. Only one model is accepted since the perfect fit with the definition expressed in Eq. (4.1) which is a matrix constraint (Stewenius et al., 2006) often used for determining the essential matrix, which E denotes the essential matrix mentioned in Eq. (3.5).

$$2EE^TE - tr(EE^T)E = 0 \qquad (4.1)$$

Figure 4.1 Matching result example

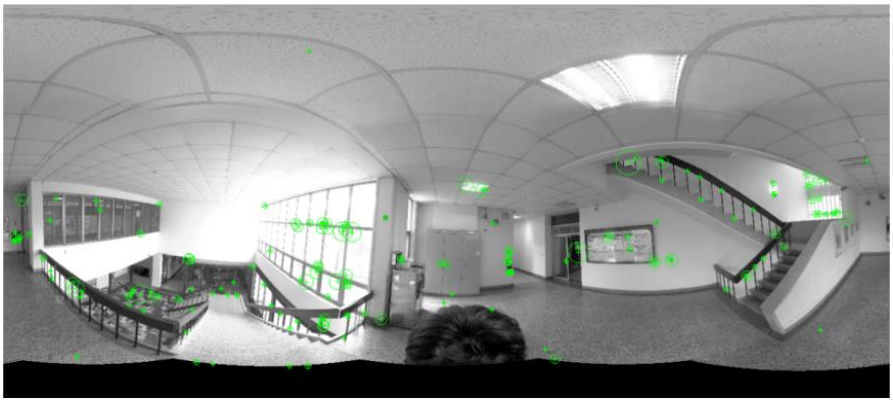

The mathematical model plays a significant role in RANSAC algorithm. It is the criterion to distinguish the inliers and outliers of the data. For frame image, the relationship between two images can be described by affine transformation. With this transformation relationship, the conjugate points can be filtered. This can be achieved by transforming the coordinates of one image to another as described in Eq. (4.2).

$$\begin{bmatrix} x_p^B \\ y_p^B \end{bmatrix} = \begin{bmatrix} \cos\omega & \sin\omega \\ -\sin\omega & \cos\omega \end{bmatrix} \begin{bmatrix} m_x & m_y \sin\alpha \\ 0 & m_y \cos\alpha \end{bmatrix} \begin{bmatrix} x_p^A \\ y_p^A \end{bmatrix} + \begin{bmatrix} \Delta x \\ \Delta y \end{bmatrix} \qquad (4.2)$$

The geometry relationship of SPI is different with frame images. Because of the complicated geometry, affine model cannot be used for eliminating error matching. A reasonable way is find a suitable transformation model. In this study, essential matrix is applied to be the transformation model. The transformation model is shown as Eq. (4.3).If the matching pair is correct, it will satisfy the coplanar condition.

$$\begin{bmatrix} x_p^A \\ y_p^A \\ z_p^A \end{bmatrix}^T \begin{bmatrix} e_{11} & e_{12} & e_{13} \\ e_{21} & e_{22} & e_{23} \\ e_{31} & e_{32} & e_{33} \end{bmatrix} \begin{bmatrix} x_p^B \\ y_p^B \\ z_p^B \end{bmatrix} = 0 \tag{4.3}$$

Figure 4.2 The flow chart of RANSAC for elimination.

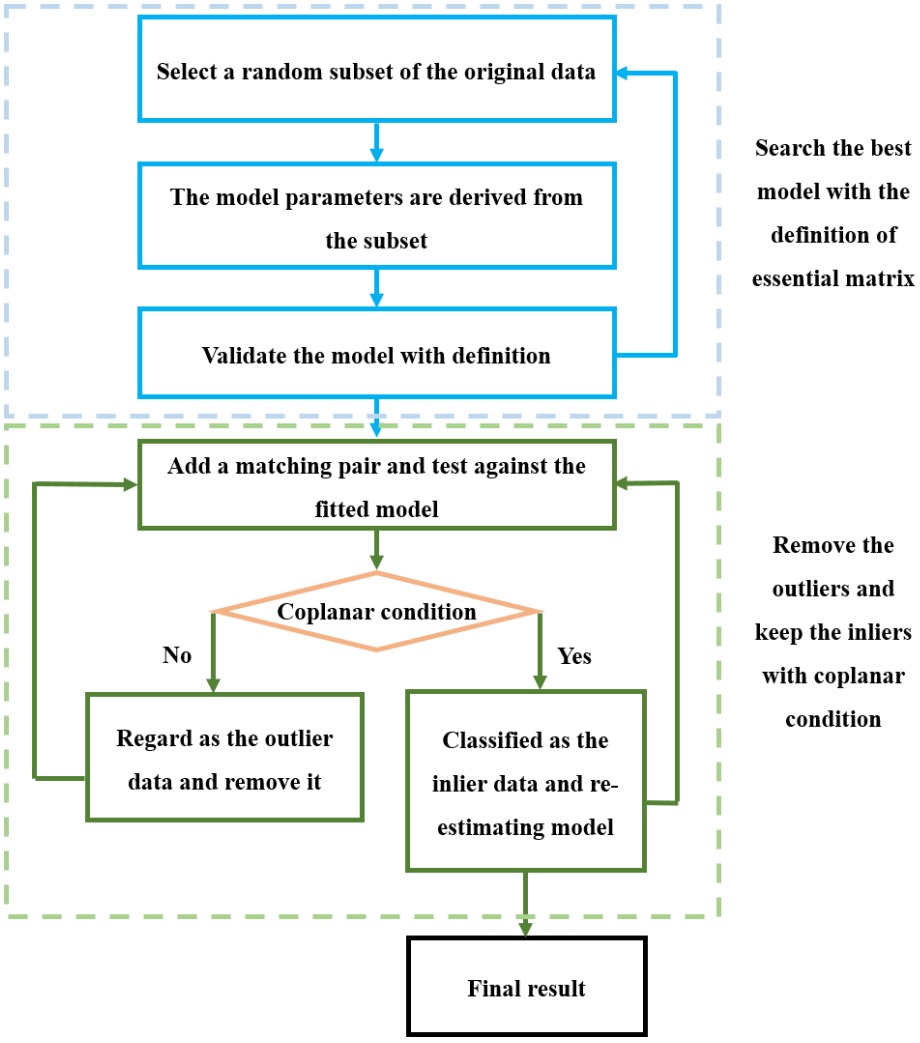

5. EXPERIMENT RESULT AND ANALYSIS

5.1. Essential Model Test

An experiment was conducted to compare affine and essential models for the cases of translate, rotate and tilt of the station. Each case involves several SPIs. Five images (A1~A5) were tested in the translation test; four images (B1~B4) were tested in the rotation test; and three images (C1~C3) were tested in the tilt test. Table 5.1 ~ 5.3 show the result with respect to the three test cases.

Figure 5.1 Matching result of movement test.

(a) Affine Model (b) Essential Model

Figure 5.2 Matching result of self-rotation test.

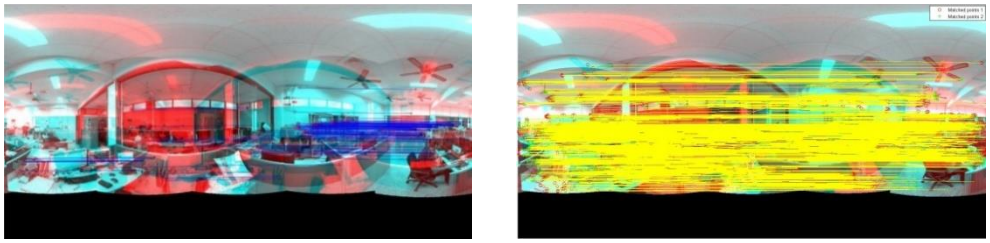

(a) Affine Model (b) Essential Model

Figure 5.3 Matching result of tilt test.

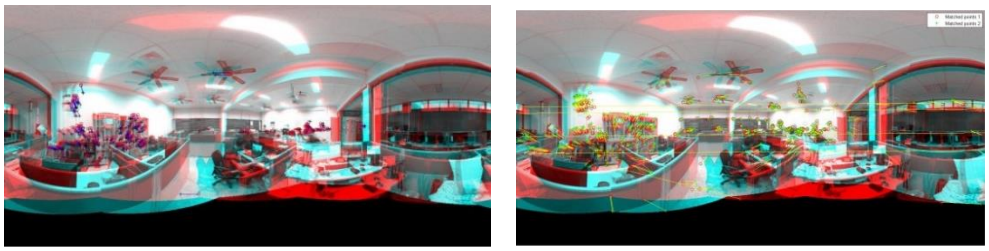

(a) Affine Model (b) Essential Model

Table 5.1 shows the numbers of pints in translation test. The number of candidate points for each image pairs are all more than 400. The percentages of remaining numbers of point with RANSAC affine model are about 30%. When the essential model is applied, the percentages can be increased up to about 75%.

Table 5.1 Comparison of affine and essential model in movement test.

	A1A2	A2A3	A3A4	A4A5
Number of candidate matches	404	413	466	500
Number of remaining matches after RANSAC with affine model	130 (28%)	128 (31%)	139 (30%)	190 (38%)
Number of remaining matches after RANSAC with essential model	360	335	330	410

Table 5.2 shows the numbers of points in the rotation test. The numbers of candidate points for each image pairs are all more than 1800. The percentages of remaining numbers of point with RANSAC affine model are about 40%., the percentages can be increased up to about 95 % using essential model.

Table 5.2 Comparison of affine and essential model in self-rotation test.

	B1B2	B2B3	B3B4	B4B1
Number of candidate matches	1888	1836	1891	1870
Number of remaining matches after RANSAC with affine model	680 (36%)	624 (34%)	794 (42%)	766 (41%)
Number of remaining matches after RANSAC with essential model	1831 (97%)	1762 (96%)	1834 (97%)	1776 (95%)

Table 5.3 shows the numbers of points in the tilt test. The numbers of candidate points for each image pairs are all more than 700. The percentages of remaining numbers of point after RANSAC process with affine model are about 30%. When the essential model is applied, the percentages can be increased up to about 90%.

Although essential model performs much better than affine model in RASNAC algorithm for SPI cases, there are still very few matched points distributed in the top and bottom area due to the serious image distortion. Even if SURF can detect the feature points in these areas, feature descriptions of these corresponding

points will differ from each other, and will be removed in SURF matching. To solve the problem, it is necessary to cope with the image distortion generated by projection.

Table 5.3 Comparison of affine and essential model in tilt test.

	C1C2	C2C3	C1C3
Number of candidate matches	1119	1384	760
Number of remaining matches after RANSAC with affine model	358 (32%)	525 (38%)	212 (28%)
Number of remaining matches after RANSAC with essential model	1040 (93%)	1301 (94%)	554 (73%)

5.2. Relative Orientation Test

The indoor environment of Dept. of Geomatics contains two floors and stairs, 18 control points are measured by total station for calculating E.O. parameters of SPIs, and there are seven check points used to validate the result. Fifteen SPIs were captured using Ladybug 5 system. Fig. 5.4 shows the distribution of control points, check points and image stations. Image matching was performed to find corresponding points between two overlapped SPIs. Fig. 5.5 shows the example of matching results of two SPIs, the red point means the matching feature point.

Figure 5.4 Distribution of control points.

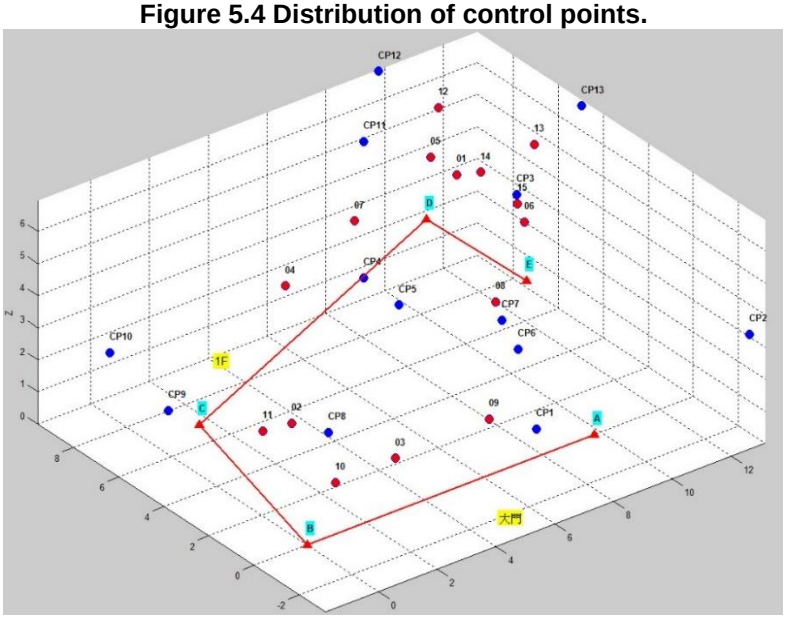

Figure 5.5 SPI No. 1 match with SPI No. 14 (192 matching points)

(a) SPI No. 1

(b) SPI No. 14

Five images were chosen for testing, they were called query SPIs in the following statement, relative orientation parameters were computed to determine the POPs of SPIs using other ten control SPIs. Two test cases were done in this study. In test case I, manual measurements of corresponding points were applied to ensure the quality of matching pairs; the test case II is the overall test with the use of automatically measurements of corresponding points determined by SURF and RANSAC algorithm. Table 5.4 shows the difference compare to the results, also the mean errors and RMSEs.

Table 5.4 Coordinate errors and mean errors and RMSEs of case I.

	Case I			Case II		
SPI	**△X(m)**	**△Y(m)**	**△Z(m)**	**△X(m)**	**△Y(m)**	**△Z(m)**
1	**-0.002**	**0.027**	**-0.004**	**0.011**	**-0.005**	**-0.016**
2	**-0.007**	**0.001**	**0.002**	**0.448**	**-0.315**	**0.464**
3	0.045	0.007	0.014	0.216	-0.030	0.050
4	0.302	0.052	0.126	-3.654	4.090	-0.097
5	0.040	0.038	0.002	0.138	-0.276	0.060
Mean Error	0.076	0.025	0.028	0.203	-0.157	0.140
RMSE	±0.137	±0.031	±0.057	±0.258	±0.201	±0.235

The case I results show errors less than a few cm except SPI No. 4. This reveals the importance of the quality of corresponding points. The coordinate errors of SPI No. 4 are larger than the other four SPIs, especially the X coordinate. For mean error and RMSE in Case II, SPI No. 4 is not taken into account. Comparing the results of test case II with case I, coordinate error increase obviously. The much larger errors resulted from improper matching pairs of corresponding points generated from automatic matching process. Except SPI No. 4, coordinate errors of all other SPIs are still under 1 meter.

The test of SPI No. 4 is the worst case in both Case I and Case II. In test case II, the coordinate errors even reach to four meters. By checking the distribution of control SPIs shown in Fig 5.6, SPI No. 4 locates at the stairs and there are few control SPIs around it. Table 5 shows the numbers of corresponding points between each query SPI and the top three control SPIs in the test case II. Much fewer conjugate points were found for query SPI No. 4. This reveals that the number of corresponding points also effects the positioning result. On the other hand, the distribution of matched points in query SPI No. 4 is mainly on the X direction, which may cause the situation of unbalanced geometry. Based on the observations, both the quantity and the distribution of corresponding points are also important factors for the computation.

Table 5.5 Numbers of corresponding points between overlapped SPIs.

	Matched SPI and number of corresponding points					
SPI No. 1	SPI No. 14	297	SPI No. 5	175	SPI No. 15	91
SPI No. 2	SPI No. 11	154	SPI No. 4	33	SPI No. 9	32
SPI No. 3	SPI No. 10	149	SPI No. 9	72	SPI No. 2	46
SPI No. 4	SPI No. 1	28	SPI No. 7	22	SPI No. 10	20
SPI No. 5	SPI No. 1	191	SPI No. 14	79	SPI No. 15	60

Table 5.5 give the results of the relative rotation matrix of SPI No. 3, and the validation data are also given. By checking the results of test case I with the validation data, the calculated rotation matrix is an acceptable. For example, comparing the result of case I and case II in Table 5.6~5.8, the respective elements of computed rotation matrix are similar to those validation data, which means the result of SPI No. 3 can be considered as reasonable orientation.

Table 5.6 relative rotation matrix and rotation angles of SPI No. 3.

True value			
Rotation angle	**ω**(˚)	**φ**(˚)	**κ**(˚)
	2.09	5.34	2.05
Relative rotation matrix	0.9999500	0.0092206	-0.0024579
	-0.0092417	0.9999200	-0.0087257
	0.0023773	0.0087480	0.9999600

Table 5.7 relative rotation matrix and rotation angles of SPI No. 3.

Case I			
Rotation angle (with SPI No.10)	ω(˚)	φ(˚)	κ(˚)
	0.14	4.92	-8.24
Relative rotation matrix (with SPI No.10)	0.9914800	-0.1476800	-0.0888930
	0.1435900	0.9978000	0.0275950
	0.0856700	-0.0024022	0.9932500
Rotation angle (with SPI No.9)	ω(˚)	φ(˚)	κ(˚)
	-0.29	5.29	-7.13
Relative rotation matrix (with SPI No.9)	0.9938100	-0.1292400	-0.0944780
	0.1243800	1.0024000	0.0208890
	0.0921150	0.0050840	0.9910100

Table 5.8 relative rotation matrix and rotation angles of SPI No. 3.

Case II			
Rotation angle (with SPI No.10)	**ω(˚)**	**φ(˚)**	**κ(˚)**
	-0.13	2.18	-2.40
Relative rotation matrix(with SPI No.10)	1.0017000	-0.0416810	-0.0376630
	0.0419840	0.9999100	-0.0067668
	0.0381130	0.0022535	1.0018000
Rotation angle (with SPI No.9)	**ω(˚)**	**φ(˚)**	**κ(˚)**
	-0.95	6.10	-4.54
Relative rotation matrix (with SPI No.9)	1.0011000	-0.0829180	-0.1079900
	0.0795190	1.0013000	0.0072074
	0.1062900	0.0165310	0.9995200

6. CONCLUSION

In this study, we combined the SURF and RANSAC algorithm for searching the overlapped SPIs and measuring the corresponding image features automatically. Essential matrix which based on coplanar condition is applied in RANSAC algorithm to cope with SPI matching process. With essential matrix, the efficiency and reliability of matching results are more robust. Once the matching is done, the position and orientation parameters (POPs) between two overlapped SPIs can be computed with essential matrix again. A novel solution of intersection ambiguity of SPI while calculate the relative orientation is also proposed and get a good result.

Two test cases including manual and automatic measurements of corresponding points are compared. For positioning result, using manual measurement can provide the coordinates error less than a few centimeters. About coordinate error is about twenty centimeters while using the automatic measurements. It reveals the incorrect matching pair is the main reason causing the poor position result. It means that the computation of position relies very much on the data quality of corresponding points. According to the results, fewer conjugate points will lead to an unreasonable position of unknown SPI. It means that the numbers of corresponding points also effects the positioning result.

For orientation computation, we may get reasonable results, but it may result in unreasonable numbers sometimes. The experiment results do not show a reliable and stable solution for relative rotation. At the present stage, we still cannot give a clearly conclusion about why the results are unstable. What we can confirm so far is that the measurement errors of corresponding points will affect the orientation results based on the test of simulated data.

7. REFERENCE

Bay, H., T. Tuytelaars, and L. Van Gool (2008). SURF: Speeded Up Robust Features, *Computer Vision and Image Understading,* 110(3), pp. 346-359.

Fischler, M.A. and R.C. Bolles (1981). Random Sample Consensus: A Paradigm for Model Fitting with Applications to Image Analysis and Automated Cartofraphy. Comm. Of the ACM, Vol. 24, pp. 381-395.

Hayet, J.B., F. Lerasle and M. Devy (2007). A visual landmark framework for mobile robot navigation. Image and Vision Computing 25, pp.1341-1351.

Hartley, R. and A. Zisserman (2004). *Multiple View Geometry in Computer Vision,* Cambridge Univ., pp.257-260.

Horn, B.K.P. (1990). Recovering baseline and orientation from essential matrix. *MIT AI Memo*.

Jyoti Joglekar and Shirish S. Gedam (2012). Area Based Image Matching Methods – A Survey. *International Journal of Emerging Technology and Advanced Engineering*, V ol. 2 Issue 1, pp.130-136.

Lienhart, R. and J. Maydt (2002). An Extended Set of Haar-like Features for Rapid Object Detection. *IEEE ICIP,* Vol. 1, pp.900-903.

Lee, Y., S. Lee, D. Kim and J.K. Oh (2013). Improved Industrial Part Pose Determination Based on 3D Closed-Loop Boundaries. *IEEE International Symposium on Robotics (ISR),* pp.1-3.

Longuet-Higgins, H.C. (1981). A Computer Algorithm for Reconstructing a Scene from Two Projections. *Nature,* 293(10), pp.133-135.

Lin,K.Y. (2014). *Bundle Adjustment of Multi-station Spherical Panorama Images with GPS Positioning,* Department of Geomatics, National Cheng Kung University, Taiwan.

Nguyen, V.V, J.G Kim and J.W Lee (2011). Panoramic Image-Based Navigation for Smart-Phone in Indoor Environment. *Springer-Verlag, Berlin Heidelberg,* pp.370-376.

Nister, D. (2004). An Efficient Solution to the Five-Point Relative Pose Problem. *IEEE Transaction on Pattern Analysis and Machine Intelligence*, 26(6):758-759.

Ressl, C. (2000). An Introduction to the Relative Orientation Using the Trifocal Tensor. *International Archives of Photogrammetry and Remote Sensing*, Vol. XXXIII, Part B3:769-776.

Stewenius, H., C. Engels, D. Nister (2006). Recent Developments on Direct Relative Orientation. *ISPRS Journal of Photogrammetry and Remote Sensing, 60(*4), pp. 284-294.

Scaramuzza, D. and F. Fraundorfer. (2012). Visual Odometry: Part I - The First 30 Years and Fundamentals. *IEEE Robotics and Automation Magazine,* 18(4), pp.85-87.

Se, S., D.Lowe and J, Little (2002). Global Localization using Distintive Visual Features. *IEEE/RSJ International Conference on Intelligent Robots and Systems,* pp.226-231.

Wahbeh W., C. Nardinocchi (2015). Toward the Interactive 3D Modelling Applied to Ponte Rotto in Rome. *Nexus Network Journal (2015)*, 17:55-71.

Zhang, Chi J. Xu, N. Xi, Y.Y Jia and W.X. Li (2012). Development of an Omni-direction 3D Camera for Robot Navigation. *IEEE/ASME International Conference on Advance Intelligent Mechartronics,* pp.262-267